Tunnelling in fault zone
Nuclear waste repository, influence of permeability

Matthias Wojnarowicz, MSc Civil Engineer, PhD Student
Laboratory of Experimental Rock Mechanics, École Polytechnique Fédérale de Lausanne

Nowadays, high hazardous nuclear waste treatment is a predominant environmental issue for all nuclear-power-generating countries, as they produce more and more nuclear waste over time with no effective method to dispose them. Radioactivity naturally decays over geological times, so radioactive waste has to be isolated and confined in appropriate disposal facilities for a sufficient period until it no longer poses a threat to the populations and environment. The current approach, for high-level radioactive waste, is deep geological disposal. A deep geological repository is a nuclear waste repository excavated deep within a stable geologic environment, that is suited to provide a high level of long-term isolation and containment without future maintenance. Potential rock types being considered for geological disposal including The Opalinus Clay (OPA). In Switzerland, the Mont Terri site was chosen for a landfill study, based on the accessibility and stratigraphy which allowed the installation of an international research centre dedicated to hydrogeological, geochemical and geotechnical investigations of OPA. However, the Mont Terri complex is intersected by fault zones, witch can leads to potential hazards. The elements that result from this study are intended to be applied to a nuclear landfill site.

The main objective of our study is to find an optimum solution for a deep burial project, by using numerical simulations. This study focuses on the effect of anisotropy induce by the bedding planes and the fault itself. To do this, we will vary the initial conditions such as the depth and pore pressure, within the range of the study of Mont Terri's formations.

ISSUES RELATED TO TUNNELLING IN FAULT ZONES – MONT TERRI CASE STUDY

Fault zones excavations issues

Faults are long zones of complex deformation, forming areas of discontinuities in the mineralogical and mechanical properties together with hydrogeological conditions. They are generally generated in the Earth's upper crust. The pattern of shear and tensile fractures reflects the orientation of the principal stresses due to the tectonic forces. The crushing of brittle rock and the reorientation of grains by shearing, generates fine grained gouges. Brittle fault zones consist of randomly occurring units of more or less undeformed rock called ”horses”, with a lenticular shape surrounded by fine grained gouges. Those extreme contrast in stiffness between block and matrix leads to heterogeneous displacement and secondary stress distribution along the tunnel, both during the excavation and at long term. On top of that, groundwater conditions may change drastically across the fault.

Fault zones at Mont Terri are complex structures due to the high heterogeneous rock mass conditions and permeability. The presence of faults can generates high displacements, stability problems, and groundwater inflows. Besides the difficulties of such conditions, long-term security is a major problem for radioactive disposal. Displacement due to tectonic forces need therefore be monitored over time.

Definition of the principal issues to be addressed is based on the study of the following document (see reference [1]).

The Opalinus Clay case

Clay formations are considered to be well suited for radioactive wastes as a result of its low hydraulic conductivity and self-sealing capabilities. Clay also provides good sorption capacity for radionuclide transport. Clay properties vary according to the water content, it behave as a brittle rock at low values and as soft ductile material at high values. Clay minerals typically form over long periods of time as a result of the gradual chemical weathering of rocks and some sedimentary depositing. They form a layer stack which gives it an anisotropic behaviour. The deep geological disposal of nuclear waste in Opalinus Clay, is currently being assessed, in Switzerland, Mont Terri research center. The Underground Rock Laboratory (URL) is located in Jura's Canton. The access is provided through the security gallery of the mont Terri tunnel along the A16 motorway connecting Biel to Porrentruy. Mont Terri's URL is located in a 90 m thick sequence of OPA. The average overburden is around 300 m deep. The excavation axis is approximately parallel to the strike of the bedding plane (139/33; strike/dip). The bedding plane has been shown to affect the mechanical response of the rock by inducing strong directionality on its deformation, strength and hydraulic properties.

The Mont Terri's URL is characterized by three different fault systems: (i) moderately SSE-dipping reverse faults, (ii) low angle SW-dipping fault planes and sub-horizontal fault, and (iii) moderately to steeply inclined N to NNE-striking sinistral strike-slip faults.

In order to define the characteristics of our model, we make reference to five documents (see reference [2, 3, 4, 5, 6]).

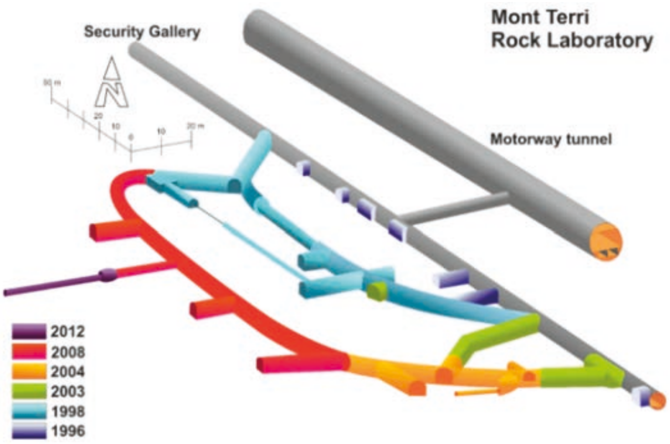

Fig. 1. Mont Terri Rock Laboratory diagram

MODELLING OF THE EXCAVATION

Model properties

The parameters provides by the Mont Terri's URL are summarized in the table 1.

For simplification, we used a value of E = 7 GPa for the rest of the article. The evaluation of the in-situ stress field is difficult because of the strong anisotropy behaviour of clays, such as OPA, and it has to be determined using some numerical analysis in laboratory, and in situ works. The results are presented in the following table.

To model a potential nuclear repository, we use a finite element mechanics software called Lagamine. The model used in a 2D mesh with a 1.5 m radius excavation and a fault passing by the excavation with a 45 degrees angle. The principal stress σ_1 is σ_v due to the overburden of rock mass from above. The bedding plan is set at a 30 degrees angle with respect to the horizontal. We use different elements geometries and characteristics to characterise the fault gouge, the fault core, and the rest of the model. They are all Q8 elements, 8 mechanical nodes and 8 fluids ones. They provide a quadratic motion function, thus a linear variation of the stress field by elements. The mesh is denser close to the excavation and near the fault in order to give us a better approximation of deformation and stress.

Constitutive law (equilibrium):

$$\nabla\sigma + f = 0 \tag{1}$$

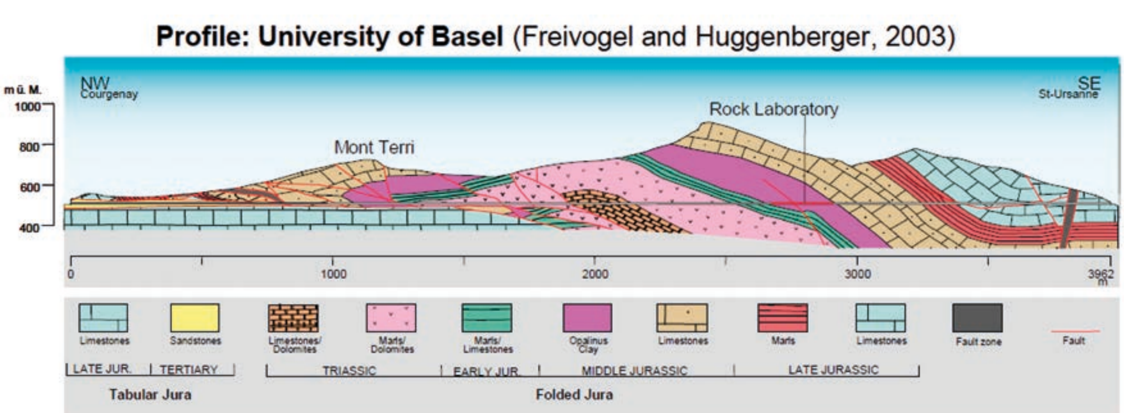

Fig. 2. Geological profile with rock laboratory position

Table 1. Properties of OPA (see reference [5])

Property	Value
Elastic modulus drained (shallow oedometer S-specimens), E_{ds} [GPa]	2
Elastic modulus drained (deep oedometer S-specimens), E_{dd} [GPa]	4
Elastic modulus undrained shallow (oedometer S and P-specimens), E_{us} [GPa]	4 ÷ 8
Elastic modulus undrained deep (oedometer S and P-specimens), E_{ud} [GPa]	9 ÷ 18
Poisson's ratio parallel to bedding, ν_p	0.35
Poisson's ratio perpendicular to bedding, ν_s	0.25
Shear modulus perpendicular to bedding, G_s [GPa]	3.7
Uniaxial compressive strength parallel to bedding, UCS_p [MPa]	11.6 ± 3.9
Uniaxial compressive strength perpendicular to bedding, UCS_s [MPa]	14.9 ± 5.1
Indirect tensile strength parallel to bedding, T_p [MPa]	1.30
Indirect tensile strength perpendicular to bedding, T_s [MPa]	0.67

Table 2. Stress field on the faults (see reference [5])

Principal stress	Orientation	Trend [°]	Plundge [°]	Magnitude range [MPa]
σ_1	Sub-vertical	210	70	6 ÷ 7
σ_2	NW-SE	320	7	4 ÷ 5
σ_3	NE-SW	0.52	18	2 ÷ 3

Table 3. Permeability

Parameters	Value
K_{para}	$5e^{-20}$
K_{perp}	$5e^{-21}$
K_{fault}	$5e^{-19}$

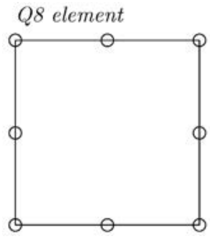

Fig. 3. Model FE with "Q elements" to characterise the fault

Table 4. Envelope of yield criterion bedding

Mohr Coulomb failure envelope	ϕ' [°]	C'_0 [MPa]	C'_{45} [MPa]	C'_{90} [MPa]	ν	E [MPa]	G [MPa]
OPA shallow (up to 400 m)	19	1.3	0.85	1.7	0.27	7000	2756
OPA deep (400-900 m)	24	2.9	1.95	3.9	0.27	7000	2756

Table 5. Envelope of yield criterion matrix

M-C envelope	ϕ' [°]	C' [MPa]
up to 400 m	29	3.1
400-900 m	33	7.1

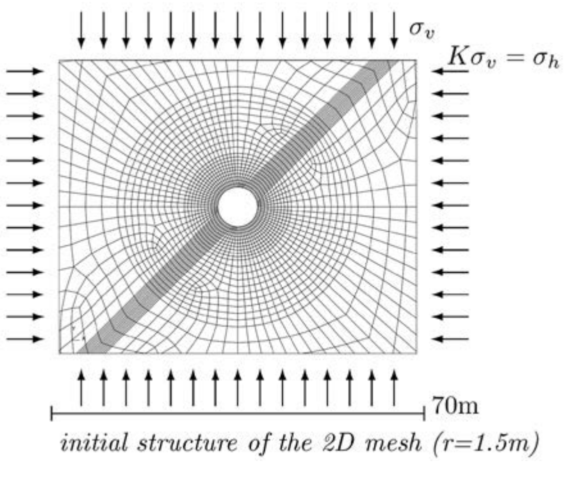

Fig. 4. 2D mesh model

Interpretation of the results

Homogeneous case

In a first step, we perform an isotropic case in order to compare them to the Kirsch elastic solutions and the elastoplastic solution. This allows us to verify the validity of the model. We chose to include pore pressure in the calculation of the effective pressure, but with no drainage. We choose an overburden of 300 m, and a pore pressure of 2 MPa, thus a σ'_v = 6.15 MPa (see table 5 for others parameters). This value of σ'_v will be retained until the final case, in order to compare the influence of each parameters on the model. To compute the Kirsch solution we took K_0 = 1. The Kirsch solution for the excavation are given in the table 6.

Table 6. Stress and displacement at the limit of the excavation, elastic solution

	σ_x	σ_y	$U_{x,y}$
$x = r / y = 0$	0 MPa	12.3 MPa	1.7 mm
$y = r / x = 0$	12.3 MPa	0 MPa	1.7 mm

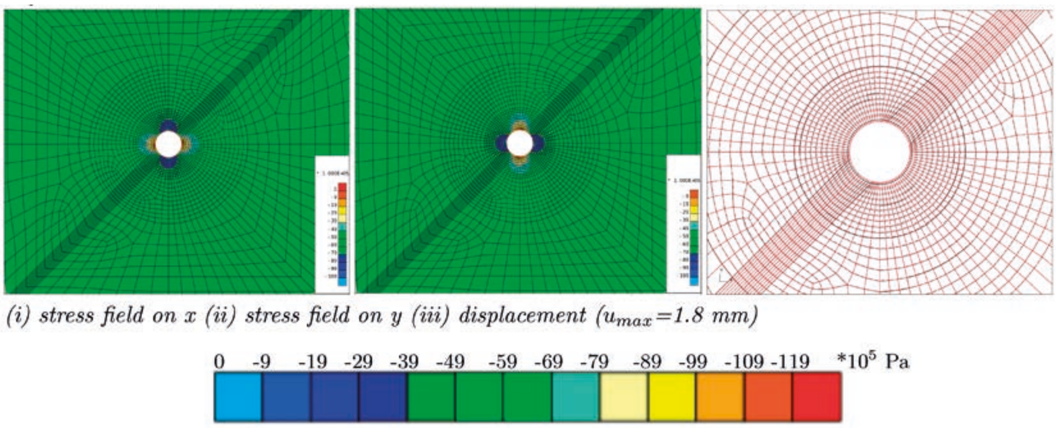

Fig. 5. Stress redistribution and displacement, isotropic case.

The elastoplastic solution, which assumes that the rock behaviour is elastic perfectly plastic, is presented in the table 7 (see equations (1) to (4)).

Table 7. Stress and displacement at the limit of the excavation, elastoplastic solution.

	σ_x	σ_y	$U_{x,y}$
$x = r / y = 0$	0 MPa	10.5 MPa	2.4 mm
$y = r / x = 0$	10.5 MPa	0 MPa	2.4 mm

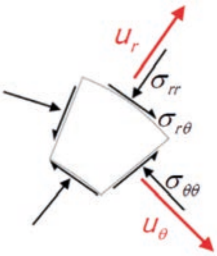

Fig. 6. Principal stresses after excavation

Due to the excavation and the fact that the pressure in the enclosure is the atmospheric one, we observe a redistribution of stresses around the excavation. Right at the limit of the excavation σ_r can be approximate to zero ($P_{at} << \sigma_i$), thus the redistribution take place on σ_θ and $\sigma_{r\theta}$ (figures 5 and 6). Thereafter we plot on the same graph, the deformation at a distance *R* from the centre of the excavation obtained from the elastic, elastoplastic and numerical solutions. As we can see on the graphs (figures 7 and 8), the numerical and analytical solutions gave us similar values on displacements and stresses. The plastic zone as developed until 0.06 m from the excavation surface, which explains the small difference between both of them. We can conclude on the fact that at 300 m the Kirsch elastic solution give us to a good approximation on the rock behaviour thereby it validates our model.

Elastoplastic stress in elastic zone:

$$\sigma_r = \frac{b^2 r_f^2 (P_f - P_0)}{b^2 - r_f^2} \cdot \frac{1}{r^2} + \frac{b^2 P_0 - r_f^2 P_f}{b^2 - r_f^2} \tag{2}$$

$$\sigma_\theta = -\frac{b^2 r_f^2 (P_f - P_0)}{b^2 - r_f^2} \cdot \frac{1}{r^2} + \frac{b^2 P_0 - r_f^2 P_f}{b^2 - r_f^2} \tag{3}$$

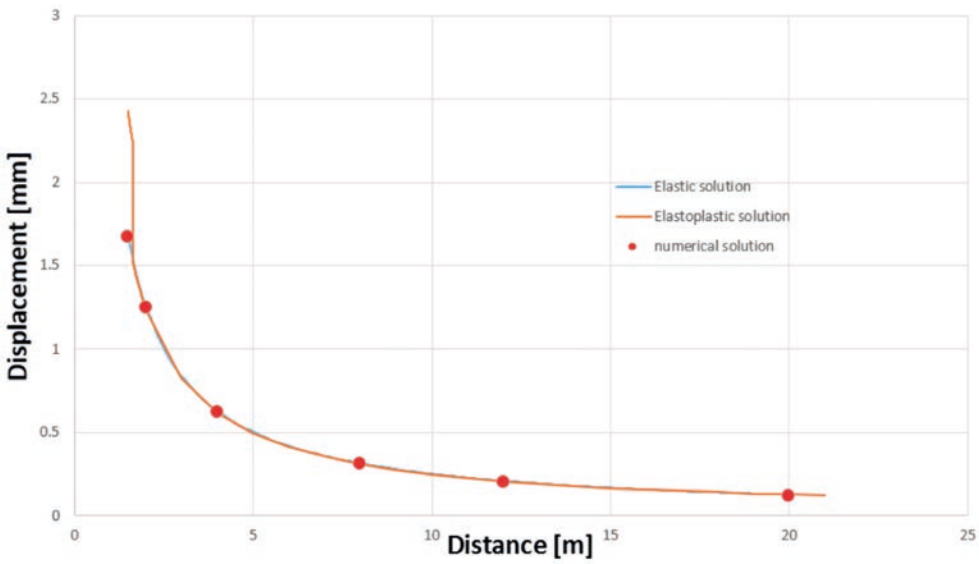

Fig. 7. Displacement at a distance *R* from the excavation

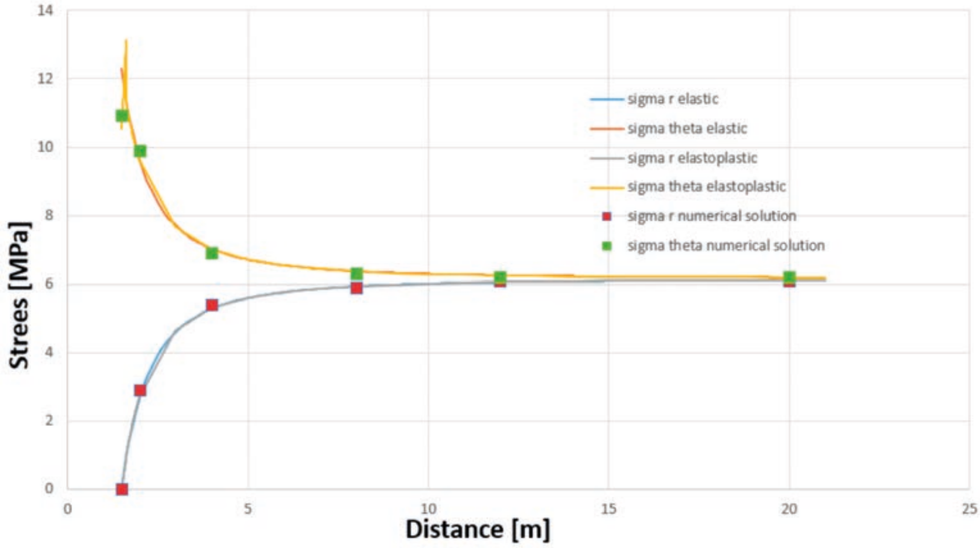

Fig. 8. Stress at a distance R from the excavation

Elastoplastic stress in plastic zone:

$$\sigma_{rp} = c \cdot \cot\phi \left[\left(\frac{r}{a} \right)^q - 1 \right] + P_i \cdot \left(\frac{r}{a} \right)^q \tag{4}$$

$$\sigma_{\theta p} = c \cdot \cot\phi \left[m \cdot \left(\frac{r}{a} \right)^q - 1 \right] + mP_i \cdot \left(\frac{r}{a} \right)^q \tag{5}$$

$$m = \frac{1 + \sin\phi}{1 - \sin\phi} \tag{6}$$

$$q = \frac{2\sin\phi}{1 - \sin\phi} \tag{7}$$

In order to compute the elastoplastic solution we study the following document (see reference [9]).

In order to see the influence of stiffness on displacements and stress, we are going to reduce it (see table 9). We can clearly see on the numerical model that the displacement vary when we change the elastic modulus (see figure 9). The displacement increases , in the other hand the stress field is pretty similar. Indeed the stress are independent of the modulus of elasticity (see equations (2)(3)(4)(5)).

Table 9. Values of elasticity

Parameters	E_1	E_2	E_3
Values [GPa]	4	5	7

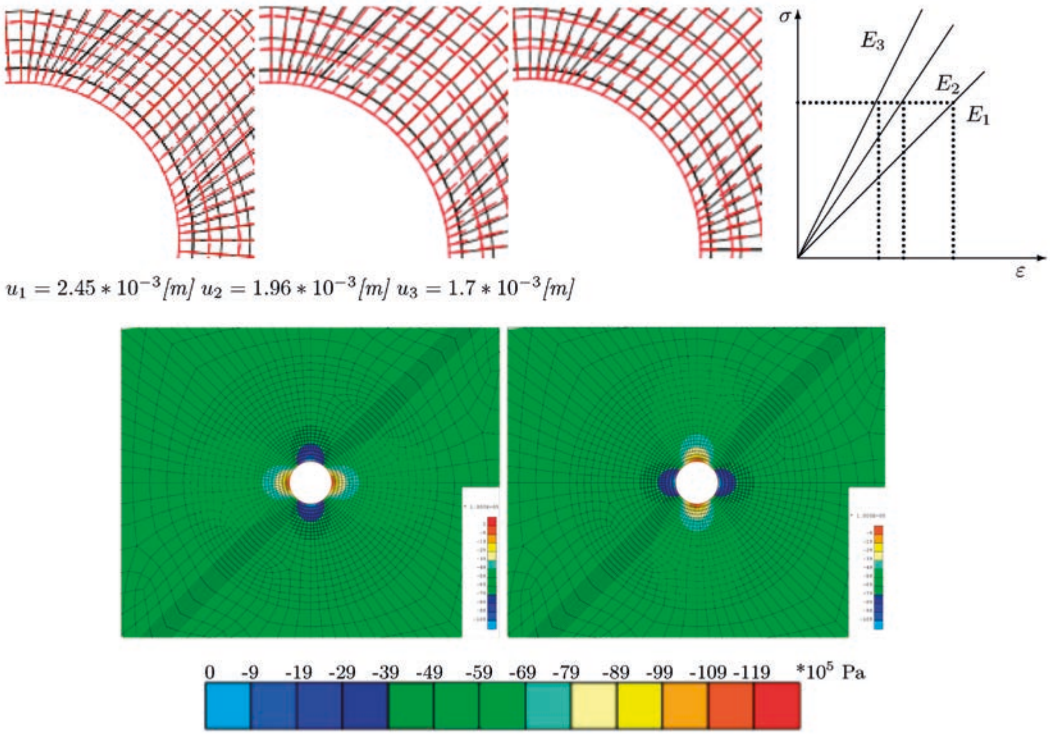

Fig. 9. displacement and stress field around the excavation

Development of pore pressure

The pore pressure can vary over a wide range during and after the excavation. We made the assumption that the rock is saturated. These local changes in pore pressure can locally modify the effective stress and can leads to differential displacement along the radial axis of the tunnel. It can also locally create sup-pressure when the soil pass from a undrained state to a drained, as we see in the part 4.2.4 (see figure 16 (ii,1) and (ii,2)). Anisotropy due to the bedding and faults should be take into consideration as they greatly influence the permeability, thereby creating differential displacement along the radial axis and the orthoradial axis. Those cases will be shown thereafter. The internal pressure after the excavation, being the atmospheric one, it form an hydraulic gradient from the soil, to the excavation. Since the excavation surface can be considered as drainage surface, groundwater inflow occurs towards the excavation, that should be taken in consideration during the construction phase and afterward for the lining design. The pore pressure develops at a logarithmical rate all around the excavation, until it reaches a stable state, as can be seen in the figure 10. Afterwards, we have a permanent flow state.

The evolution of pore pressure over time based on a numerical model for the isotropic case was shown in the figures 10 and 11.

Anisotropic case

In order to see the influence of the mechanical and hydraulic anisotropy on the excavation, we consider different values for the matrix and the bedding, as well as difference of permeabilities (see table 3 and 4).First, an analytical model is presented to understand the effect of the bedding on the mechanical behaviour of the rock. Second, as the implemantation of the bedding was not possible on Lagamine, we included just the hydraulic anisotropy in the numerical model.

Mechanical anisotropy

The bedding is inclined at 30 degrees in our model. The yield criterion on the foliation follow a Mohr-Coulomb criterion. Discontinuities represent a weaker part in a rock, thus discontinuity induce by the bedding inclination lead to differential behaviours among the rock mass (especially between the bedding plan and

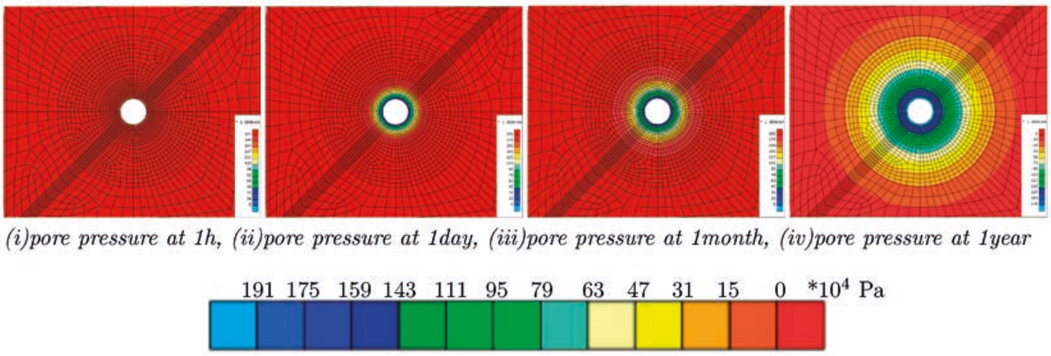

Fig. 10. Pore pressure distribution over time

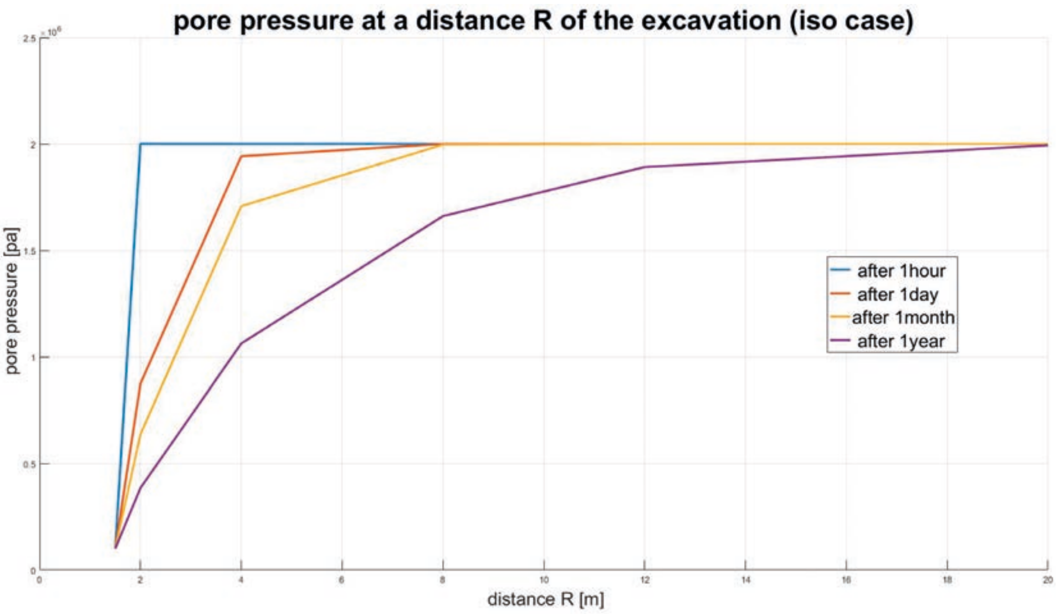

Fig. 11. Pore pressure at a distance *R* from the excavation (isotropic case)

the plane orthogonal to the foliation plane). The yield criterion for the intact rock is σ_{ci} = 14.9 MPa (UCS uniaxial compressive stress perpendicular to bedding) given by the table 1. We plot in the figure 14 (ii), the evolution of the bearing capacity σ_1 as a function of the bedding inclination. This show us that there is a preferential direction of rupture around 55° (45° + $\phi/2$) for the foliation.

$$\tau = \sigma \tan(\varphi) + C \tag{8}$$

Anisotropic rock criterion:

$$\sigma_1 - \sigma_3 = \frac{2(C_w + \sigma_3 \tan(\varphi_w))}{(1 - \tan(\varphi_w)\cot(\beta))\sin(2\beta)} \tag{9}$$

In this example we draw the envelope of Mohr-Coulomb with the uni axial compressive test and a Brazilian one, then we show for a certain as, the bearing capacity ai for the maximum angle of bedding, this leads to the formula (9).

Due to the preferential direction of failure induce by the anisotropy, the displacement should be influence by the weaker direction, thus we assist to differential displacement along the excavation. We observe an ovalization of the cavity at a 30 degrees angle, corresponding to the bedding inclination. Since we don't have a numerical solution to simulate an ubiquitous joint, we chose to estimate analytically the differential displacement by interpolate the value of cohesion at 30 degrees (c_{30} = 1.15 MPa). Then compare it to the elastoplastic solutions of a 0 degree (parallel to the bedding) and 90 degree angle (perpendicular to the bedding), by making the assumption that the deformation is perfectly ellipsoidal. Thus the anisotropy of the material is taken into account trough the material cohesion that depends on the angle between the principal stress and normal to bedding orientation (we use the cohesion value of table 4). since the cohesion decrease linearly (see figures 13 and 14), we can interpolate the displacement along the excavation surface (see equation (10)) and rotate them by 30 degrees.

Ellipse equation:

$$\left(\frac{x}{\delta_{r1}}\right)^2 + \left(\frac{y}{\delta_{r2}}\right)^2 = 1 \tag{10}$$

Table 10. Displacement for both cases

$\delta_r\,(c_{30})$	$\delta_{r2}\,(c_{90})$	$\delta_{r1}\,(c_0)$
1.7 [mm]	1.8 [mm]	1.7[mm]

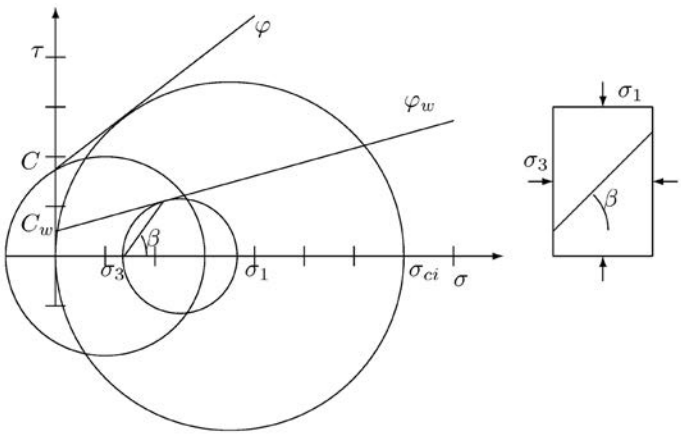

Fig. 12. Envelope of Mohr Coulomb for an anisotropic rock.

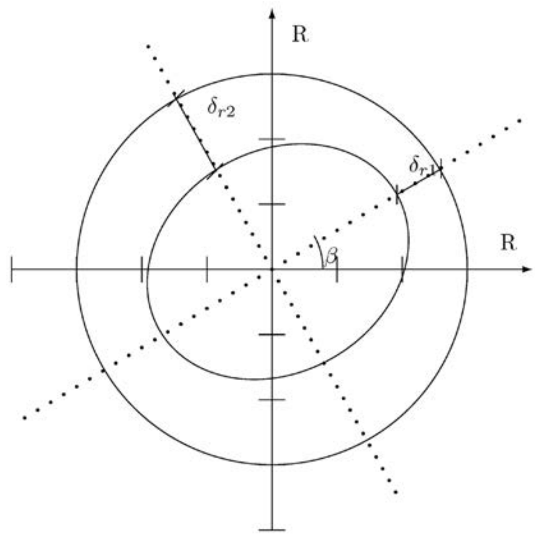

Fig. 13. Influence of hydraulic anisotropy on an hollow cylinder

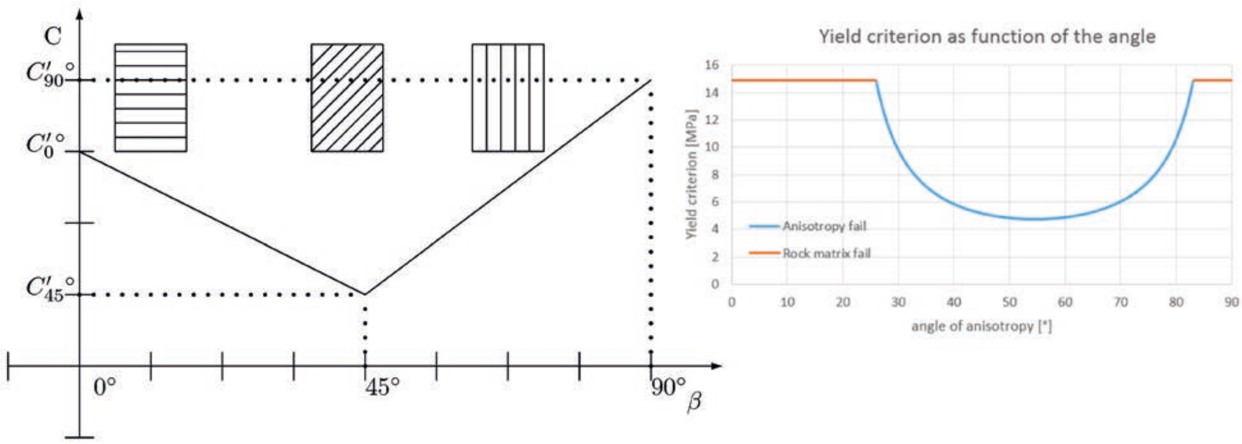

(i)cohesion as a function of the bedding inclination, (ii)bearing capacity as a function of the bedding inclination (C'=1.3 MPa, ϕ'=19 °, equation (9)).

Fig. 14. Influence of bedding inclination on cohesion and bearing capacity

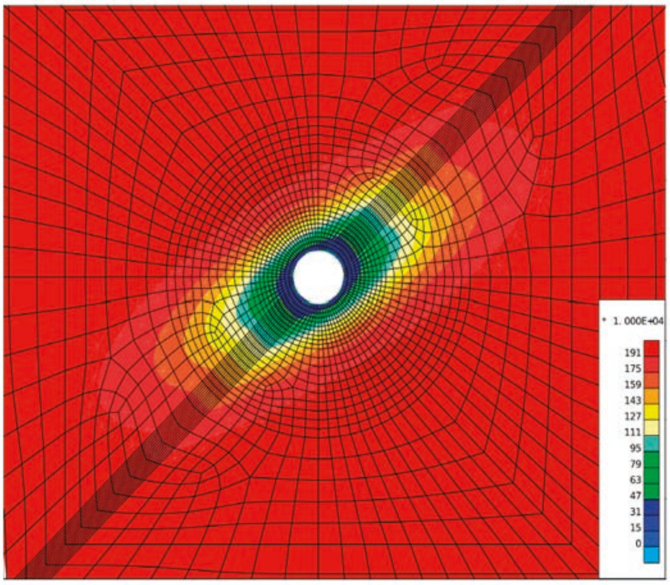

Fig. 15. Influence of hydraulic anisotropy on an hollow cylinder.

Hydraulic anisotropy

Bedding have also a large influence on the hydraulic behaviour, since each stack of layer is formed by the accumulation of eroded material, the interaction faces constitute surfaces with lower permeability. This lead to differential repartition of pore pressure. We observe an equipotential ovalization turned at 30 degree from the horizontal (as we can see in the figure 15).

This phenomena can amplified the displacement across the matrix, as pore pressure act on effective constrain.

Influence of the fault, preferential or barrier for radionuclide leakage path

A damage zone is the volume of deformed wall rocks around a fault surface that results from the initiation, propagation, interaction and buildup of slip along faults (see reference [12]). Fault zone are discontinuity in a volume of rock, across which there has been significant displacement as a result of rock-mass movement. Due to the presence of fine grained gouges with low permeability inside the fault, it leads to height or low hydraulic gradient. Thus as we saw before it generate heterogeneous stress field around the excavation. This part as for scope to show the influence of hydraulic anisotropy induce by the fault and bedding plan as well as mechanical anisotropy due to the fault.

Hydraulic behaviour of faults

We will show the pore pressure repartition around the model for different parameters of permeability, to simulate a low and high permeability fault. Thereafter we are going to add the hydraulic anisotropy induce by the bedding plan and see the influence they both have on each other. We can see zones of overpressure at early age when we couple the anisotropy induce by the fault and the bedding. This is due to the transition from non-drain to drain. We observe a preferential direction of flow in the direction of the fault orthogonal to the equipotential. When we add the hydraulic anisotropy of the bedding the leakage direction are between the fault and bedding direction (see figure 16 (ii)). Finally when the fault act as a barrier for leakage (k_f = $10^{-}21$ [m^2], lower than the matrix one), we observe a shrinkage of the equipotential at the fault, and thus permeability of the bedding is predominant (see figure 16 (iii)). It as also the effect of increas-

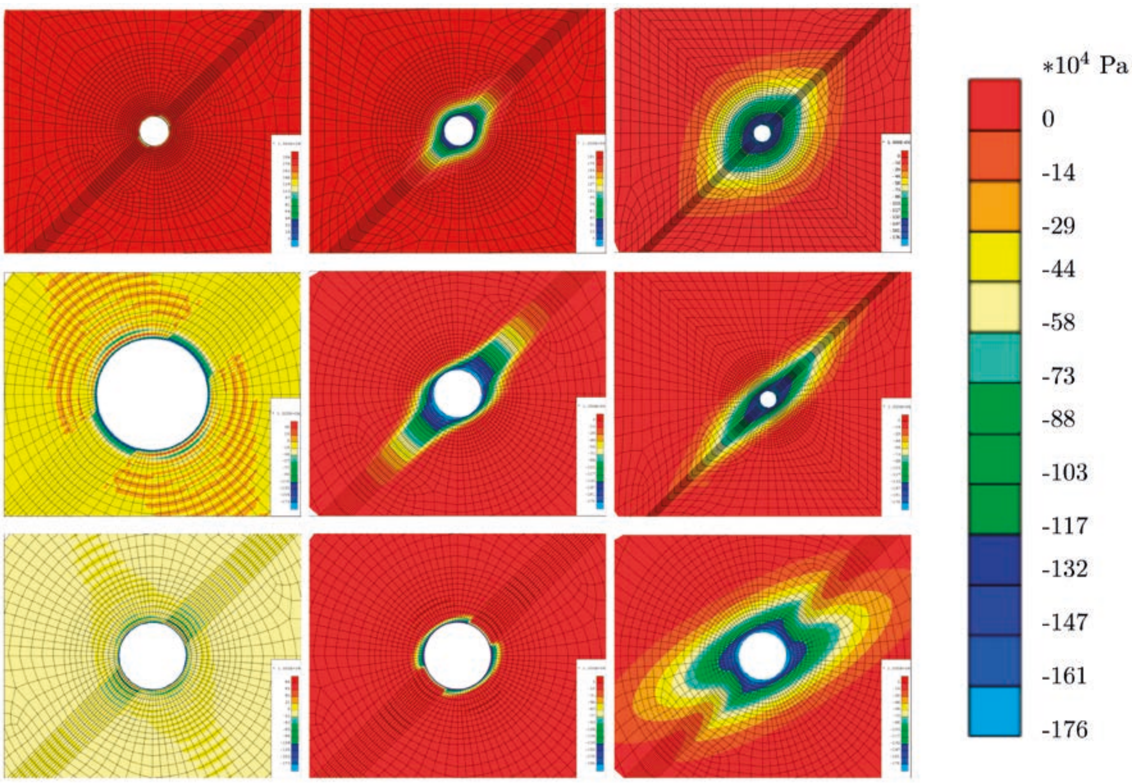

Fig. 16. Pore pressure variation induce by the fault over time

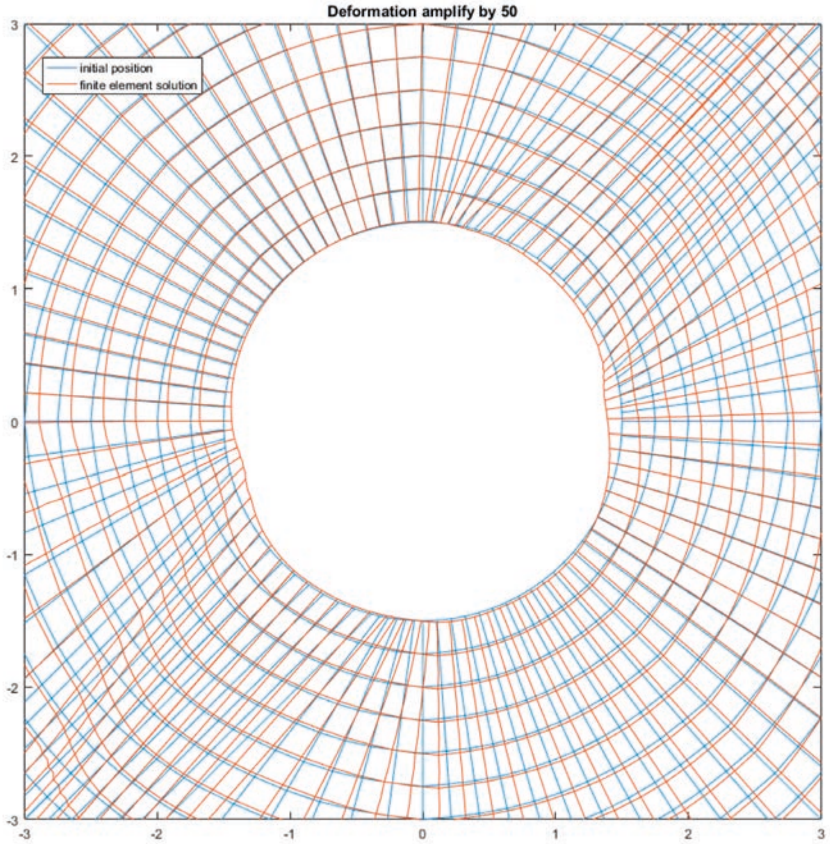

Fig. 17. Deformation for different medium

ing the time of drainage. The Mohr-Coulomb criterion of fault core and gouges is lower than the intact rock. This changes in characteristics leads to a poor interaction between the two side of the fault core (the hanging wall and footwall), thus can lead to failure by shear forces.

Mechanical behaviour of faults

For the mechanical part, we implement our own finite element code in order to get a numerical solution on displacements around the excavation surface. The present solution is an elastic solution which does not take into account a shear rupture surface, thus we have a continuity across the different medium with different values of stiffness. We consider a plane constrain problem. The presence of the fault as the effect of creating differential deformations. We observe two zones of high deformations on the excavation surface, one under the fault in the upper part, and one above the fault in the lower part (see figure 17). Those deformations seems to be induce by a stress concentration on those areas, probably due to the shrinkage of the lower stiffness mediums. With a model including a failure criterion we could assist to differential displacement of the two sides of the fault, and therefore cracking near the fault which can lead to rock mass instability.

Table 11. Elastic modulus of our model

	E_{matrix}	E_{core}	E_{gouge}
[GPa]	7	5	0.8

Final case

Due to the difficulties encounter during the modelling phase, we decide, in the latter case to confront the two models (Lagamine: hydraulic anisotropy, elastoplastic and Matlab: mechanical anisotropy, elastic). The Lagamine model give us an overview of the variations of pore pressure that occur near an excavation. Thus we can compute the deformation across the excavation axis for different depth and water table at a 0 and 45 degree angle (see figure 18). We observe a quasi-linear relation between depth, pore pressures and displacements. indeed they both act on the effective pressure. The displacements at 0 and 45 degree are really close to each others (see figure 18 and 19). It seems that the model does not take into account the pore pressures in the calculation of the displacements (permeability does not influence displacements). In order to get a good representation of time dependant displacements as a function of the effective constrain we should include the variation over time of the pore pressures in the effective constrain calculation. The Matlab model is here to show how displacements can be influence by the mechanical interaction of different medium, it include effective constrain but without coupling between pore pressure development and displacement. We study the displacement at 0 and 45 degree as for the Lagamine model. We observe a similar linear relation between the two parameters and displacement. Displacements are in the same range but are subject to more inaccuracy due to depth (since the plastic zone grow with the effective constrain). A clear difference can be observed between 0 and 45 degrees induce by the mechanical behaviour of the

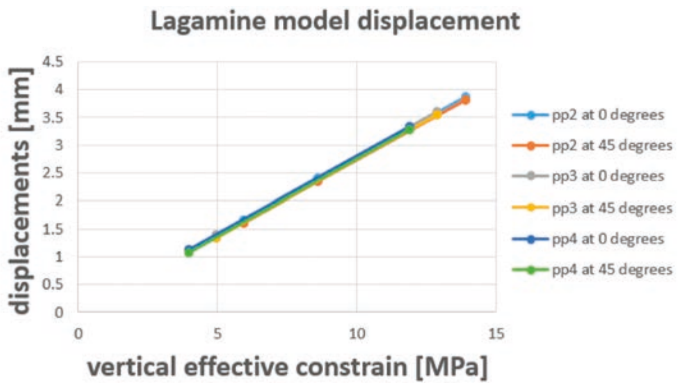

pore pressure are respectively, from left to right,
equal to 4 MPa – 3 MPa – 2 MPa
(the solution for 400 m, pp3 and pp4 does not converge)

Fig. 18. Displacement at the excavation surface for different depth and pore pressure

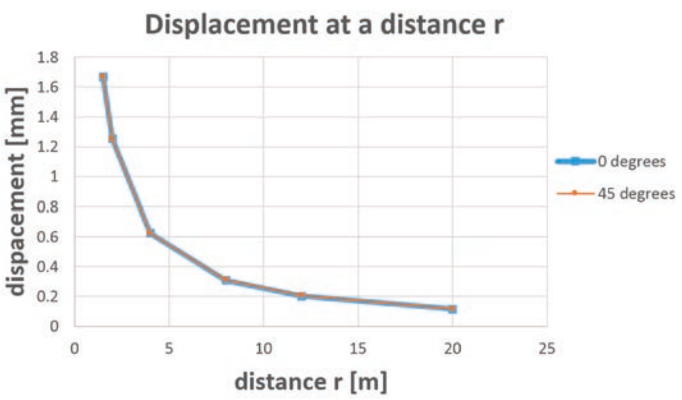

Fig. 19. Displacement at a distance r (Lagamine)

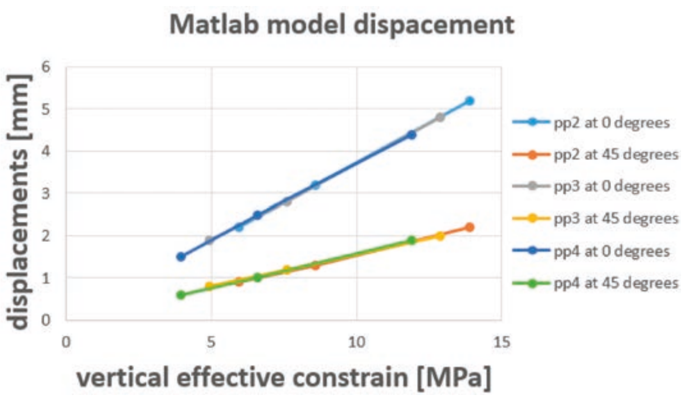

pore pressure are respectively, from left to right,
equal to 4 MPa – 3 MPa – 2 MPa

Fig. 20. Displacement at the excavation surface for different depth and pore pressure

fault (as we saw in part 4.2.4). Finally an optimum solution for a lining should be the one with the less constrain, allowing the formation of a small plastic zone, less than 5% of the radius; but should provide a sufficient depth in order to counter a possible hazardous leakage of radionuclide. A optimum solution should be around 400 m with the highest pore pressure (4 MPa). High interstitial pressure confines pollutant progression towards the exterior of the excavation. It is therefore necessary to provide drainage for decontamination or storage in case of leakage.

CONCLUSION

When tunnelling in damage zones, it is important to acknowledge the discontinuity structures of a fault as well as the rock properties around (stiffness, resistance, anisotropy and in-situ stress state). We also observed the influence of water table on the pore pressure development. Despite utmost care it is inevitable for a model to contains uncertainties due to the assumptions made on rock mass behaviour, as well as mesh discretization or boundary conditions. It is why it is very important to update the geotechnical model during the construction phase and try several models. In our case the models are limited in two different way. For the Lagamine one, we only have an elastoplastic homogeneous mechanical behaviour with pore pressure repartition, but no coupling between them. For the Matlab one we have an elastic solution with different medium, but it is no longer valid a high depth (due to a formation of plastic zones). However the study of both the models allowed us to clearly acknowledge the parameters involved in displacements and constrain, thus the dimensioning of a lining. While much progress has been made over the last decade, nuclear waste repository development is a complex task, which yet require further study.

REFERENCES

1. Schubert W., Fasching A., Goricki A.: Tunnelling in Fault Zones – State of the Art.

2. Mont-terri's Internet site: https://www.mont-terri.ch/

3. Tsang C. F., Barnichon J. D., Birkholzer J., Li X. L., Liu H. H., Sillen X.: Coupled thermo-hydro-mechanical processes in the near field of high-level radioactive waste repository in clay formations.

4. Lisjak A., Garitte B., Grasselli G., Muller H. R., Vietor T.: Tunnelling and Underground Space Technology.

5. Guayacán-Carrillo L. M. Ghabezloo S., Sulem J., Seyedi D. M., Gilles A.: Effect of anisotropy and hydromechanical couplings on pore pressure evolution during tunnel excavation in low-permeability ground. International Journal of Rock Mechanics and Mining Sciences.

6. Tsang C.-F., Bernier F., Davies C.: Geohydromechanical processes in Excavation Damaged Zone in crystalline rock, rock salt, and indurated and plastic clays – in the context of radioactive waste disposal.

7. Mechanical properties of the shaly facies of Mont Terri Opalinus Clay reported by Bock (2009).

8. In-situ stress tensor at Mont Terri rock laboratory (Corkum and Martin, 2007).

9. Chen X., Tan C. P., Haberfield C. M.: Solutions for the deformations and stability of elastoplastic hollow cylinders subjected to boundary pressures.

10. Descoeudre F.: Mecanique des roche I et II, EPFL, 1977.

11. Violay M., Sandrone F.: Mecanique des roches et de ouvrages souterrains, EPFL.

12. http://www.sciencedirect.com/science/article/pii/S0191814103001391.